https://doi.org/10.48048/tis.2022.2062

Cytotoxicity and Hemostatic One Step Green Synthesis of Iron Nanoparticles Coated with Green Tea for Biomedical Application

Raghda Abou Gabal[1,*], Dina Shokeir[1] and Ahmed Orabi[2]

[1]Mansoura Urology and Nephrology Center, Mansoura University, Mansoura 35516, Egypt
[2]Department of Physics, Faculty of Science, Mansoura University, Mansoura 35516, Egypt

([*]Correspondence author's e-mail: raghdaabogabal@gmail.com)

Received: 10 February 2021, Revised: 20 May 2021, Accepted: 6 June 2021

Abstract

Heparin and its low molecular weight are anticoagulants that prevent the formation and extension of blood clots. However, these anticoagulant causes bleeding that takes longer to stop. Here, we explore using magnetic iron oxide (Fe_3O_4NPs) coated with green tea (GTPs) as a safe and effective nontherapeutic agent for blood clotting prevention. In this work, Magnetic iron oxide coated with green tea (GT@Fe_3O_4NPs) was successfully synthesized using a simple eco-friendly green method. Green tea is employed as a green reducing and stabilizing agent. We employed this method as a new low-cost and time-consuming route. Structural, blood biocompatibility and anticoagulant properties of the (GT@Fe_3O_4NPs) were analyzed. These analyses showed that the particles were of uniform shapes and sizes of 25 - 36 nm with a coating of GTPs. The vibrating sample magnetometer (VSM) measurement demonstrated a saturation magnetization of 4.90 emu/g with negligible coercivity and retentivity, indicating the superparamagnetic behavior of the GT@Fe_3O_4NPs at room temperature. The synthesized magnetic nanoparticles were highly stable and well-dispersed in an aqueous medium through their hydrophilic coating of GTPs. Cell viability and prothrombin time (PT) showed excellent blood compatibility in addition to promising anticoagulant ability, respectively. The work offers a novel, safe nanotherapeutic agent as a substitutional for heparin. As a result, GT@Fe_3O_4NPs can compete with heparin either in hemodialysis or the treatment of thromboembolic events as it can overcome related bleeding problems to a great extent.

Keywords: Fe_3O_4NPs, GTPs, Green tea, Cytotoxicity, Prothrombin time, Anticoagulant

Introduction

Hemodialysis treatment needs anticoagulation to stop thrombosis. Heparin or its low-molecular-weight derivatives are usually utilized as anticoagulation. Unfortunately, during hemodialysis, these anticoagulants transfer to the patient's blood and increase the bleeding risk. Nevertheless, systemic anticoagulation stops using heparin in patients at high risk of bleeding [1]. Zhao *et al.* [2] explored the possibility of utilizing iron oxide nanoparticles (SPIONs) with layer-by-layer self-assembled heparin as anticoagulants for blood clotting preventio. The Hep-SPIONs exhibit comparable anticoagulant ability compared to commercial heparin and have promising magnetic properties, leading to the successful removal of the anticoagulant through pro-haemodialysis. Considering this problem, furthermore, an external magnetic field can target these nanomaterials magnetically toward the desired sites. In addition, they can be successfully removed before flowing into the human body and thus reduce the risk of bleeding markedly. As a result, Fe_3O_4NPs can be successfully used as anticoagulants for hemodialysis.

Magnetic nanoparticles (MNPs) pay attention because of their unique properties, such as being superparamagnetic [3-5]. biocompatible and biodegradable [6], and expected to be non-toxic to humans [7,8]. Furthermore, unlike bulk iron, SPIONs do not have remnant magnetization in the absence of the external magnetic field; therefore, precise remote control over their action is possible makes them also advantageous as a module of the advanced drug delivery systems. These properties make magnetic nanoparticles (MNPs) have extensive applications in the field of biomedical sciences such as catalysis [9], biosensors [10,11], targeted drug delivery [12], cell tracking [13], magnetic resonance imaging (MRI), and magnetic fluid hyperthermia [14], and many biomedical applications [15,16]. Therefore, novel and

environmentally friendly biogenic reduction/green synthesis methods are highly sought. Synthesizing the metal and metal oxide by biogenic reductin methods, which include algae [17], fungi [18], bacteria [19], and higher plant extracts, can be one of the best options for nanoparticles (NPs) [20].

Green methods are environment-friendly, cost-effective, provide good yield, and have decent reproducibility [21]. The provision of biogenic reductive materials in nature makes them an upcoming prospect for the synthesis of NPs. In addition, green tea extract contains high polyphenolic compounds. These biomedical applications of green tea are mainly due to its functional groups (Polyphenols/ Caffeine), which act as capping agents in a green single-step process besides hindering the oxidation of Fe^{2+} ions by oxygen of air in the synthesizing Fe_3O_4 NPs by the co-precipitation process [22].

Shahwan *et al.* [23] produced iron nanoparticles using extracts of green tea leaves (GT-Fe NPs). The GT-Fe NPs tend to form asymmetrical clusters and demonstrate some dispersion, with particle sizes ranging roughly between 40 and 60 nm. In addition, GT-Fe NPs showed higher dye removal percentages and faster kinetics when used as a fenton-like catalyst [23]. Hussain *et al*. [24] synthesized Superparamagnetic Fe_3O_4 nanoparticles coated with green tea polyphenols (GTP), i.e., Fe_3O_4@GTPs NPs by wet-chemical method with eco-friendly. These particles displayed a high adsorption capacity (7.25 mg/g) to remove methylene blue (MB) dye in wastewater treatment. Furthermore, the particles could be easily separated from the medium by magnetic separation and potentially reused in multiple cycles.

Khan *et al.* [25] assessed the cytotoxic effects of Fe_3O_4 MNPs in normal IMR-90 lung fibroblasts. Their study exposed normal cells to various concentrations of Fe_3O_4 MNPs (1 - 100 µg/mL) for 24 and 48 h Their findings showed that Fe_3O_4 MNPs had no cytotoxicity significance on normal IMR-90 human lung fibroblasts. Namvar *et al.* [26] evaluate the *in vitro* cytotoxic activity of Fe_3O_4 MNPs that synthesized the 1-step green method using brown seaweed (*Sargassum muticum*) aqueous extract. Their findings showed that Fe_3O_4 MNPs had no cytotoxicity in a normal Chang liver cell line, providing new opportunities for safe delivery of Fe_3O_4 MNPs and anticancer therapy applications. Here, we report GT@Fe_3O_4NPs as a promising blood compatibility-superparamagnetic-nanotherapeutic for blood clotting prevention and then separating them before transfusing the blood back to the body by an external magnetic field, thus avoiding bleeding risks to restricted content.

Materials and methods

Iron (II) chloride hydrate ($FeCl_2.4H_2O \geq 98$ % extra pure, purchased from LOBA CHEMIE PVT.LTD.03486, Mumbai, India). Sodium hydroxide (Sodium hydroxide pellets AR assay 99.5 %, MW.40.00, SO. 55592, Egypt), trypan blue, phosphate buffer solution (PBS, Ph 7 phosphate, B-01868, Mumbai, India), Hanks balanced salt solution (HPSS) (1X W/ Phenol red and sodium bicarbonate, TL 1003, India), ESR tubes contain 3.8 % buffered Lithium Citrate solution (0.129 mol/L)(INTERMEDIA, EGYPT). TUVAC coagulation tubes contain buffered trisodium citrate solution concentration of either 0.109 mol/L (3.2 %); TUVAC tube internally is sprayed with 12 to 30 international units of lithium heparin. All the aqueous solutions are prepared using triple distilled deionized water, and all the chemicals are used without further purification.

Synthesis of Fe NPs and application experiment

The synthesis of magnetic iron nanoparticles using green tea extracts as described previously [27,28]. In this work, we prepared the green tea extract by soaking 60.0 g L^{-1} green tea (commercial Brand) overnight then the extract was vacuum-filtered. Separately, a solution of 0.10 M $FeCl_2 \cdot 4H_2O$ was prepared using 19.9 g of solid $FeCl_2 \cdot 4H_2O$purchased from (LOBA CHEMIE PVT.LTD.03486) 1.0 L of deionized water. Consequently, 0.10 M $FeCl_2 \cdot 4H_2O$ solution was titrated to 60.0 g L^{-1} green tea in a 2:3 volume ratio. Following this, 1.0 M NaOH solution was added until the pH was 6.0, and the formation of MNPs was marked by the appearance of an intense black precipitate. The iron particles were then separated first by vacuum-filtered water from the iron solution and then by drying it overnight a room temperature.

Furthermore, green tea reduces the usage of an inert atmosphere that is typically required to avoid the oxidation of Fe^{2+} by air. In addition, polyphenols/caffeine are the main constituent of biopolymers in green tea extract and be strong stabilizers enabling increased biocompatibility. However, these polyphenolic compounds are biodegradable, non-toxic, and water-soluble at room temperature, proving green tea extract as an effective reducing agent compared to other extracts. Further, they confer chemical functionality to nanostructures such as Fe_3O_4 MNPs [29].

Ultraviolet-visible spectroscopy (UV-Vis)

UV-Vis absorption was measured in the wavelength local of (200 - 900 nm) using a spectrophotometer (Pg instruments, T80+, UV/Vis spectrometer, China) to study the structure of specimens and their optical properties. It includes the spectroscopy of photons in the UV- visible and adjacent (near-UV and near-infrared). In this range of the electromagnetic spectrum, molecules undergo electronic transitions. As molecules have bonding and non-bonding electrons (n-electrons) can absorb energy in the form of ultraviolet or visible light to excite these electrons to higher anti-bonding molecular orbitals [30].

X-ray diffraction (XRD)

X-ray diffraction measurements of MNPs are carried out using a diffractometer (Shimadzu, XRD-6000 - Japan). The source consisted (CuKα radiation, λ = 0.15405 nm, 2 KW). It is used to determine crystallinity, structure imperfections, crystallite size, and texture. The x-ray diffraction (XRD) patterns were recorded from 4 to 100 ° in 2θ at a scanning rate of 0.02 min^{-1}. The dried powder is mounted on a sample holder with smooth double-sided adhesive tape. Many different natural structures of iron oxide, such as Fe_3O_4, α-Fe_2O_3, γFe_2O_3, Fe_2O_3, and β-FeOOH, exhibit magnetic properties [31]. The nature of the prepared Fe_3O_4 particles determined by XRD. The crystallite size D of a particle can be estimated according to the Scherrer equation $D = k\lambda/ \beta\cos \theta$. Here, the x-ray wavelength λ is 0.154 nm, k is the structure factor, which is assigned a value of 0.89, D is the average diameter of the crystals, θ is the Bragg angle in degrees, and β is the full-width at half-height of the prominent peaks [32].

Fourier transform infrared (FTIR)

FTIR spectra are analyzed with an FTIR spectrophotometer (PerkinElmer-99075, German) using the standard KBr pellet technique in the spectral range 4000 - 450 $cm^{-1}$with a resolution accuracy of 4 cm^{-1}. Fourier transform infrared (FT-IR) spectroscopy is used to identify the functional groups of the active components responsible for synthesizing GT @Fe_3O_4 NP_S [33].

Transmission electron microscopy (TEM)

Transmission electron microscopy (JEOLJEM-2100, Japan) attached to CCD camera at an acceleration voltage of 200 kV. The samples will be diluted 10 times and negatively stained before TEM measurements due to the poor conductivity of organic samples. First, a copper grid will be placed on the wax plate. Then a drop of diluted nanosuspension prepare for TEM measurements will be added to the surface of the copper grid. Moreover, a drop of 2 % phosphotungstic acid solution will also be added to the wax plate. After drying in the air, the copper grid will be placed on the top surface of the spreading phosphotungstic acid dispersion to dye for 5 min before TEM measurements [34].

Field emission scanning electron microscopy (FE-SEM)

The field emission scanning electron microscopy (FE-SEM) (JEOL JSM - IT 100, Japan) technique gives more details about the morphology of the surface and size distribution of the synthesized magnetic nanomaterials. Sample glazed with a thin layer (1.5 - 3.0 nm) of gold or gold-palladium at 20 kV and 30 μA in order to increase its conductivity [35].

Energy-dispersive x-ray (EDX) microanalysis

The structure of Fe_3O_4NPs was characterized by an energy-dispersive x-ray (EDX) spectrum using an x-ray micro-analyzer (silicon drift detector with 129 eV resolution energy) attached to (JEOL JSM IT-100) scanning electron microscope (SEM) to confirm the presence of iron in the particles, as well as to detect the other elementary compositions of the particles [36]. The GT@Fe3O4 NPs were scattered onto adhesive carbon tapes supported on metallic disks, and their images and elemental contents were recorded at different magnifications [37].

Zeta potential

The zeta potential of magnetite suspension was measured at 25 °C using zeta potential analyzer/ particle sizing systems (Malvern Zetasize Nano-zs 90, USA). The scattering angle was 90 °. The magnetic nanoparticle suspensions were diluted with deionized water before measurement. During a zeta potential analysis, charged colloidal dispersions are placed into a zeta cell (glass cuvette with round apart). Under the effect of an electric field, charged particles will display specific electrokinetic effects, including electrophoresis, electroosmosis, streaming potential, or sedimentation potential, which estimates zeta potential using the principle of electrophoresis [38].

Physiochemical studie

Magnetic moment value was evaluated at room temperature (25 °C) using a Sherwood magnetic susceptibility (Sherwood Scientific, Cambridge, England) balance using Hg [$Co(SCN)_4$]. The Gouy method is more often used to measure magnetic susceptibility, in which the sample may be presented as a long rod of material, a solution, or a glass tube packed with powder. One end of the sample is positioned in a uniform magnetic field, and the other end in a very low or 0 field. However, the force observed is much larger and can be measured using a modified laboratory balance [39].

Magnetic measurements

The magnetic behavior of nanoparticle suspensions was attempted by vibrating sample magnetometer (VSM) option of a quantum design physical property measurement system (PPMS) equip (Lake Shore-7410, USA) with a superconducting 9 Tesla magnet. Hysteresis loops of sample acquired at selected temperatures in the range of 3 - 350 K, and magnetic fields ranged from – 8 to 8 Tesla [40].

Cytotoxicity and cell viability assay

Preparation of mononuclear cells

We isolated the peripheral mononuclear cells (PBMC) from whole blood using density centrifugation with Ficol-Paque. Hanks balanced salt solution (HPSS) centrifuged with (20 mL) of heparinized human blood, the resulting cell suspension transferred to a (50 mL) sterilized centrifuge tube (Falcon, NJ) with (10 mL) Ficol and centrifuged for 20 min at 90×g, PBMC remain in the upper fraction as a ring that can be isolated, and centrifuged for 10 min at 90×g, the supernatant discarded, and the remained pellets resuspended in PBS buffer at 10 °C [41]. We counted cells by a hemocytometer based on the trypan blue exclusion method. The isolated mononuclear cells were dissolved in a culture medium, seeded at a density of (100 µL: 60,000 per well) in a 96-well plate (Falcon) at an incubator with CO_2 5 % and temp 37 °C. The culture medium (L - 15, 100 i.u./mL penicillin, 100 µg/mL streptomycin, 5 mM $NaHCO_3$, and 0.5 % (insulin-transferrin-selenium (ITS)). After 24 h, a sample was added to a hemocytometer, analyzing cell viability under a microscope. The medium changed, preparing cells for the following experiments of NP exposure [42].

Human mononuclear cell culture and treatment protocol

Cell viability and Cytotoxicity evaluation of Magnetic GT@Fe_3O_4 NPs were performed by seeding approximately 6×10^4/100 µL cells (blood mononuclear cells) in flat-bottomed 96-well polystyrene coated plate at their exponential growth phase and incubated for 24 h at 37 °C in a 5 % CO_2 incubator. Each time, the plate was centrifuged in a microplate centrifuge (Thermo Scientific 50140763) at 350×g for 10 min, discarded the supernatant, and washed the cells by (PBS+FBS) followed by centrifugation again at 350×g for 10 min then discard the supernatant. Series of dilution (20, 50, 80, 110 and 140 mg/mL) of magnetic NPs in the medium were added to the plate. After 30, 120 min of incubation, trypan blue was added to each well, and the plates were incubated for a further 10 min and placed on a shaker (Vortex-Genie) for 30 min. Cell morphology characterization was assessed by taking photographs of living cells' interaction with different NPs 30 and 120 min concentrations.

Automatic coagulation analyzer

To evaluate the activity of anticoagulant activity (extrinsic pathway factors) and plasmatic coagulation time of the magnetic nanoparticles, Prothrombin time (PT) levels were measured by Compact stago[43]. It is a fully automated, benchtop, homeostasis analyzer that uses chromogenic and immunological methods. We performed tests using fresh blood samples. Platelet poor plasma was obtained by centrifuging the tubes 10 min at 2000 - 500 g; 2 mL of plasma was added in 3 different blood tube tubes (plain tube, heparin tube, and Lithium Citrate tube). Different concentrations of GT@Fe_3O_4 (0.03, 0.06, 0.09 gm) were incubated with the citrated tube. Prothrombin time (PT) levels were evaluated automatically by Compact stago by adding the corresponding reagent. Prolonged PT indicates decreasing factors of factors VII, V, X, prothrombin and fibrinogen [1].

Results and discussion

Ultraviolet-visible spectroscopy (UV-Vis)

The UV Visible spectrum of GT @Fe_3O_4 NP_S in the aqueous GT extract is shown in **Figure 1**. The UV-visible spectrum of synthesized GT @Fe_3O_4 NPs showed a strong peak in the visible region around (422 and 242) nm that may relate to the excitation of surface P = plasmon vibrations in the Fe_3O_4-NPs.

The bandgap energy (Eg) is calculated from absorption edge wavelength (λae) using Tauc's equation [15]. The Tauc method is based on the assumption that the energy-dependent absorption coefficient α can be expressed by the following Eq. (1);

$$(\alpha \cdot h\vartheta)^{1/\delta} = B(h\vartheta - E_g) \quad (1)$$

where h is the Planck constant, ν is the photon's frequency, Eg is the bandgap energy, and B is a constant. The γ factor depends on the nature of the electron transition and is equal to 1/2 or 2 for the direct and indirect transition band gaps, respectively.

The x-axis intersection point of the linear fit of the Tauc plot gives an estimate of the bandgap energy. The bandgap represents the minimum energy required to excite an electron up to a state in the conduction band to participate in conduction [44]. The bandgap of GT@Fe_3O_4 is 2.51 eV, referring that it is a semiconductor material. The electric properties of biological materials are a measure of their interaction with electromagnetic fields. While these biological effects may or may not be desirable, they should be well understood for safety regulation purposes and exploit beneficial effects to their full potential. (ex: Dielectric material can be polarized by an applied electric field, causing dielectric polarization).

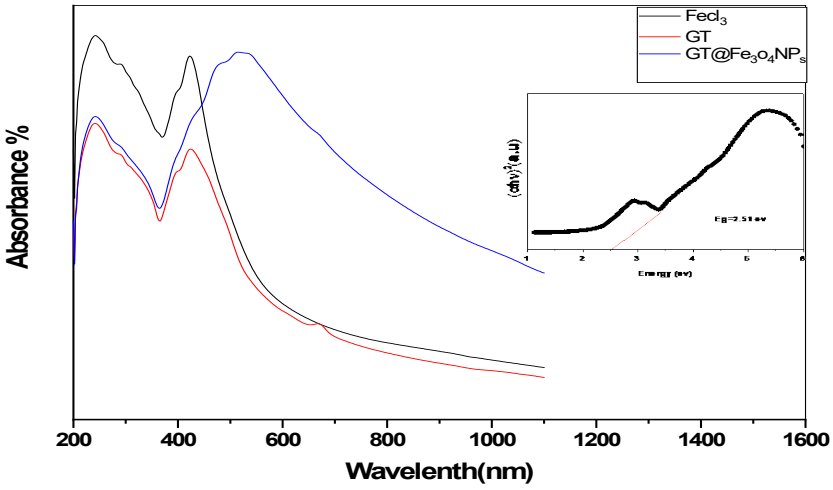

Figure 1 Uv-visible absorption spectra of iron oxide nanoparticle.

X-ray diffraction (XRD)

The x-ray diffraction patterns obtained for the GT@Fe_3O_4 NP_S synthesized using GT extract is shown in **Figure 2** are detected at 2θ = 26.64, 37.55, 43.85, 52.26, 64.34, 75.11 and 77.34 °, which are assigned to the Brag reflection of (221), (222), (400), (422), (531), (622) and (444), respectively. The analyzed diffraction peaks are matched well with the standard magnetite XRD patterns by the joint committee on power diffraction standards (JCPDS file no: 00-003-0863), which declares the crystallographic system of cubic structure. Besides, the synthesized nanoparticles are affirmed to be Fe_3O_4 but not maghemite (γ-Fe_2O_3) by comparing the XRD patterns with the standard maghemite JCPDS file no: 88-0315 [45]. A considerable difference can be seen in that the XRD patterns of γ-Fe_2O_3 consist of many peaks, unlike Fe_3O_4, which only involves few peaks. The reduction in peak intensities of GT@Fe_3O_4 NP_S is mainly due to the GTPs layer coated over Fe_3O_4 nanoparticle surfaces. Estimation of the crystallite size of synthesized Fe_3O_4-NPs can be calculated using the Debye-Scherrer Eq. (2) [46], revealing a relationship between X-ray diffraction peak broadening and crystallite size. The Debye-Scherrer equation is shown as follows;

$$D = \frac{0.94\lambda}{\beta\cos\theta} \quad (2)$$

where D is the crystallite size of synthesized Fe_3O_4-NPs for (hkl) phase, k is Scherrer constant (0.9), λ is the X-ray wavelength of radiation for Cu Kα (0.154 nm), β_{hkl} is the full-width at half maximum (FWHM) at (hkl) the peak in radian, and θ_{hkl} is the diffraction angle for the (hkl) phase. The estimated crystallite size of synthesized Fe_3O_4-NPs is 9.02 nm, calculated from the full-width at half maximum of the Fe_3O_4 the most intense peak (400) diffraction peak at $2\theta = 43.85°$ [47]. Thus, the particle size is estimated to be 9.02 nm, and this size comes within the superparamagnetic size limit of Fe_3O_4 NPs [48]. The smaller size of the coated NP_S is due to the coating of the Fe_3O_4 with GT surface, which may inhibit the growth of the particles [49].

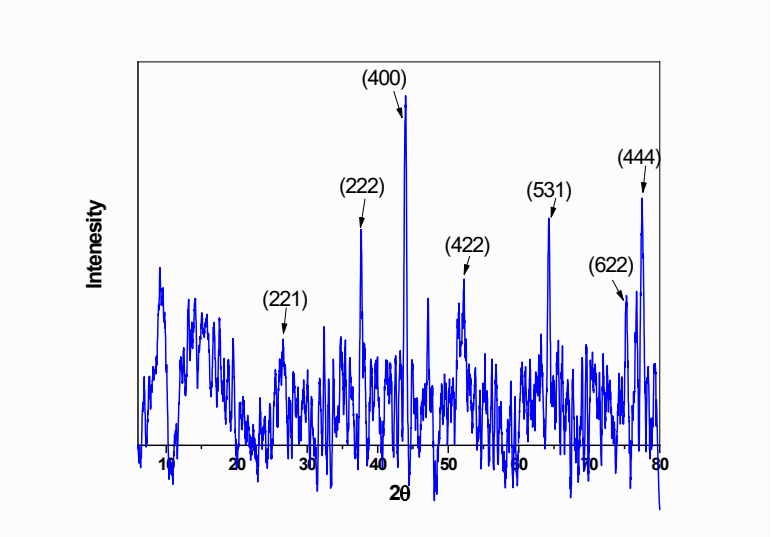

Figure 2 XRD patterns of Synthesized GT@Fe_3O_4 NPs.

Fourier transform infrared (FTIR)

FTIR spectrum of synthesized GT @Fe_3O_4 NP_S as shown in **Figure 3**. The intensities of transmittance vary due to the interaction of metal ions with GT bio compounds, which leads to the reduction and stabilization of the Fe_3O_4 nanoparticles [50]. The synthesized GT @Fe_3O_4 NP_S absorption bands around at 3748, 3268, 2395, 2270, 2179, 2040, 1608, 1413, 1016, 856, 780, 633 and 564 cm^{-1}. The absorption peak at 3286 cm^{-1} in the GT @Fe_3O_4 NP_S is attributed to the O - H stretching vibration. The absorption peaks at 2395 cm^{-1} attributed to the C–H stretching vibrations of the $–CH_2$ functional group. The absorption peaks at 2270 cm^{-1} are attributed to the C = N stretching. A band at 1608 cm^{-1} reveals carbonyl groups C = C (1550 - 1650 cm^{-1}) [51]. The presence of these functional groups confirmed that flavonoid and terpenoids molecules coated the surface of Fe_3O_4 [52]. The peaks at 1413 and 1016 cm^{-1} revealed the asymmetric and symmetric stretching vibration of COO-. The absorption peak of 856 cm^{-1} and 780 confirmed the presence of an aromatic C-H bending band. The absorption peaks found at 633 and 564 cm^{-1} in the spect are associated with Fe-O's stretching vibration mode [53]. The metal-oxygen band at 564 cm^{-1}corresponds to intrinsic stretching vibrations of metal at the tetrahedral site related to the magnetite phase of magnetite nanoparticles is observed in HI Saleh [54].

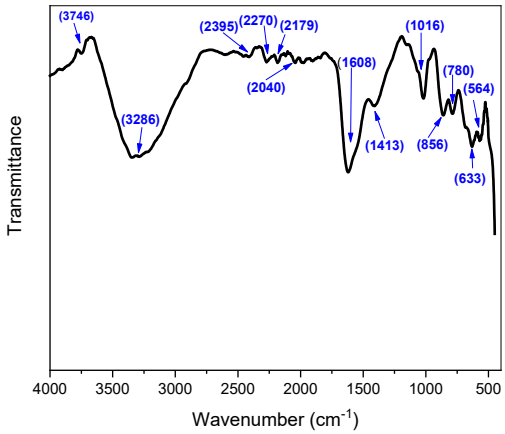

Figure 3 FT-IR spectra of synthesized Fe_3O_4@GT NPs.

Transmission electron microscopy (TEM)

The morphology and size of the synthesized GT @Fe_3O_4 NP_S were evaluated by TEM, as shown in **Figure 4a**. It showed that GT @Fe_3O_4 NP_S formed in the nanoscale and spherical shape where the particle size average between 25 nm to 36 nm. The particle size revealed by TEM is more remarkable than estimated by XRD, as the particle size analyzed by TEM is for Fe_3O_4 coated with GTPs, but the particle size estimated by XRD is measured from the Fe_3O_4 lattice parameter. The image showed the agglomeration of the particles, which might be due to hydroxyl groups or the extract thickening properties of green tea. Besides, the tendency of agglomeration is not as unexpected as the synthesized Fe_3O_4@GT NP_S has a small size and magnetic characteristic. A few tiny spherical objects can be found in the image, which might be due to the residue of green tea.

The selected area electron diffraction (SAED) pattern recorded on a single particle s of the coated NPs is shown in **Figure 4b**. The electron diffraction patterns showed a set of rings of spots mainly originated from the crystal planes of the nanoparticles, in which rings marked as (1) - (3) can be related to (444), (222), and (400) planes of the randomly orientated cubic inverse spinel structured Fe_3O_4. The appearance of these distinct diffraction rings also confirmed the polycrystalline nature of the nanoparticles.

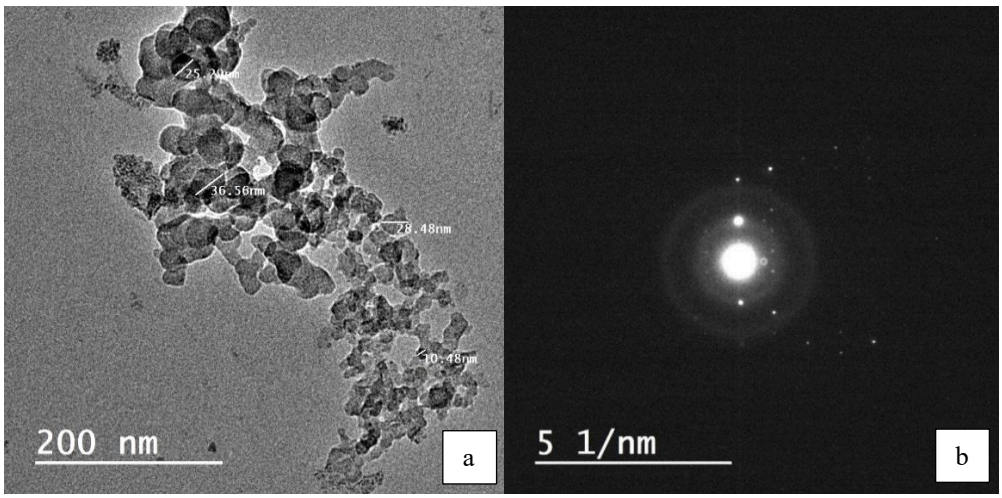

Figure 4 TEM images of Magnetic Fe_3O_4@GT NPs.

Field emission scanning electron microscopy (FE-SEM)

Typical FE-SEM images of GT@Fe_3O_4 showed in **Figure 5**. FE-SEM images revealed that the surface is rough. Surface roughening may be due to the deposition of polyphenolic compounds around the core material. In addition, particles get aggregated to the various extent that might arise from the interaction of magnetic dipole moment particles between the particles [42].

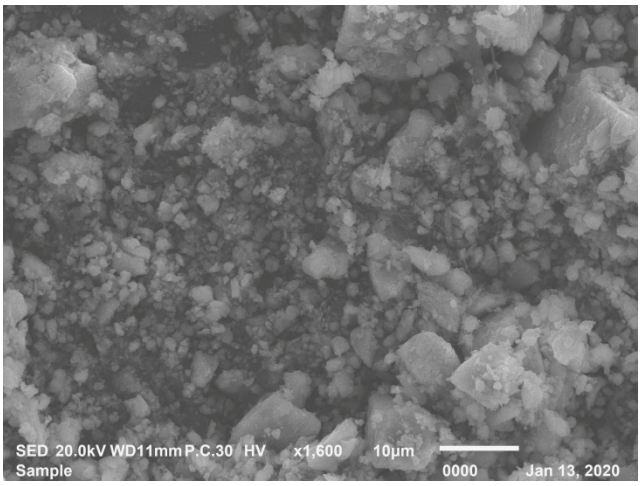

Figure 5 FE-SEM images of Magnetic GT@Fe_3O_4 NPs.

Further, information regarding the chemical composition of the GT@Fe_3O_4 was obtained with the help of EDX spectroscopy. The presence of Fe, C, and O in the EDX survey spectra of the green tea-coated magnetite nanoparticles confirm the existence of the green tea shell around the super magnetic core. In addition to these 3 distinct peaks of chloride and copper substantiated the successful immobilization of functionalizing groups or chemical residues.

EDX microanalysis confirms the presence of iron, oxygen, and carbon with an atomic percentage of37.32, 36.49 and 21.06 %, as shown in **Figure 6**. In addition, a strong signal at 6.2 was found, and an optical absorption peak at 0.5 KeV attributed to Fe is observed that confirmed the presence of Fe_3O_4 NP_S. The C group is attributed to the polyphenolic groups and other C- containing groups that proved coating Fe with GT.

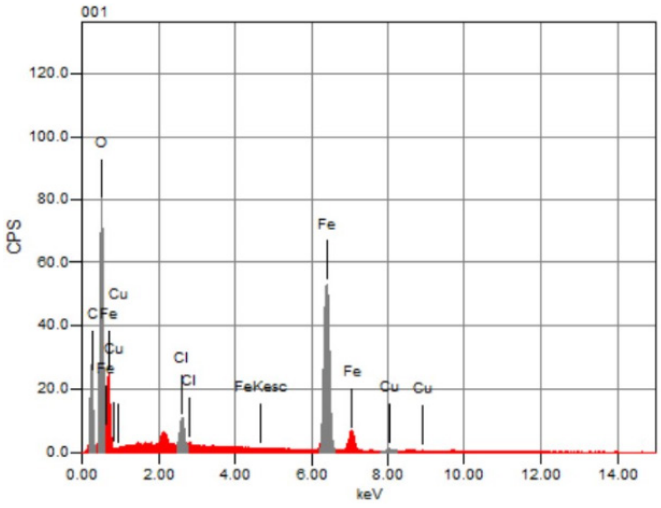

Figure 6 EDX analysis of Fe_3O_4@GT NPs zeta potential.

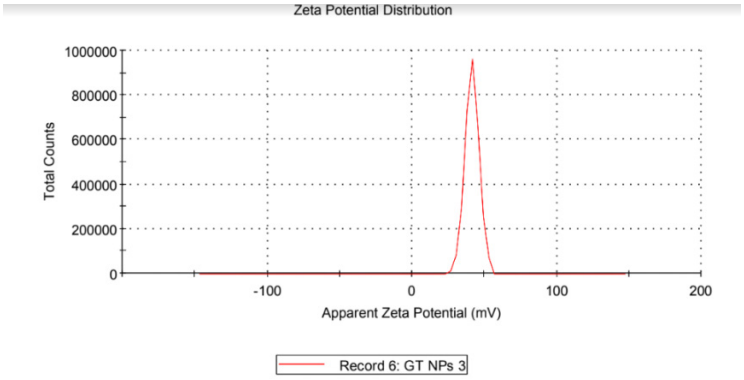

Figure 7 Zeta Potential analysis of GT@ Fe_3O_4 NPs.

The zeta potential of Fe_3O_4 prepared exhibited 41.4 mV with a standard deviation of 4.91 is shown in **Figure 7**. This significant zeta potential indicates relatively high positive charge density on the surface of nanoparticles because of the surface coating with GT that generates repulsive forces between nanoparticles. Nano particles with zeta potentials more positive than +30 mV or more negative than -30 mV usually are considered stable. The positively charged surface of synthesized MNPs compared with chemically synthesized MNPs proved that our MNPs coated with GT bio compounds. Negatively charged surfaces can more easily initiate thrombotic events because, in physiological coagulation, platelet contact with an anionic surface starts the coagulation cascade [55].

Therefore, another critical consideration when evaluating new nanomaterials. Initially, several authors had shown that protein adsorption decreased after the functionalization of the nanomaterial as the hydrophobicity of the nanoparticle's surface was also decreased [56]. In addition, the binding of nanoparticles to plasma proteins such as albumin can increase biological properties that reduce the complement system's activation, increase blood circulation time and reduce toxicity [57].

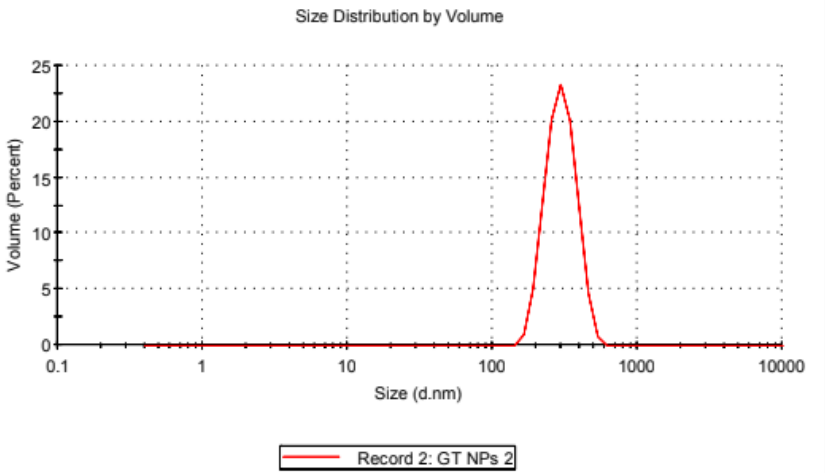

Figure 8 DLS of GT@ Fe_3O_4NPs.

The average particle sizes obtained by this technique are much larger than those by TEM, especially for magnetic Fe_3O_4 nanoparticles. As even in the absence of an external magnetic field, the magnetostatic (magnetic dipole-dipole) interactions between the particles can cause their agglomeration [58]. The DLS of magnetite nanoparticles prepared to have 1 particle size class, as shown in **Figure 8**. The average size of MNPs obtained by DLS is higher than that observed in TEM, possibly due to non-uniform size distribution and aggregation of MNPs in solution.

Magnetic measurements

Estimation of the magnetic moment of synthesized GT@Fe_3O_4NPs can be calculated from the magnetic susceptibility using Eq. (3), which reveals a relationship between the magnetic moment and molar susceptibility [59].

$$\mu_{m=}\frac{(R-R_o)*L*C}{(W-W_o)*10^9} \quad (3)$$

where μ_m is the magnetic moment of synthesized GT@ Fe_3O_4 NP_S, X_m is molar susceptibility, and T is the temperature (25 °C). Using the equation, the estimated magnetic moment of synthesized Fe_3O_4-NPs is 3.82 BM.

We study the magnetic behavior of GT@Fe_3O_4 NP_S, magnetization measurements performed with vibrating sample magnetometry (VSM). As can be observed in **Figure 9**, the specific saturation magnetization value is measured to be 4.9374 emu/g for GT@ Fe_3O_4 NP_S. The negligible coercivity Hc of hysteresis loop and consequently no remanence Mr indicated the superparamagnetic nature of the GT@ Fe_3O_4 NP_S. The formed magnetic nanoparticles within the GT should be smaller than 25 nm, and they might be considered to have a single magnetic domain. However, it should be noted that despite reducing the Msvalues, it showed the ease of separation from the reaction mixture.

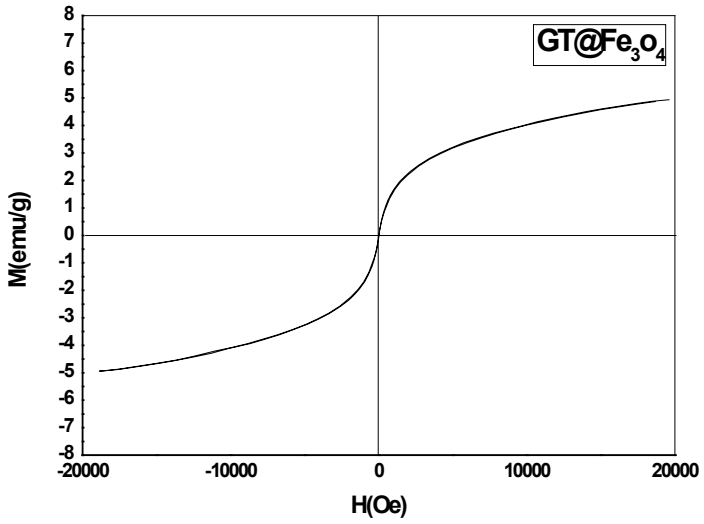

Figure 9 Magnetization curve of GT@Fe_3O_4 NPs.

Cytotoxicity and cell viability assay

The collected mononuclear cells, either after insulation or 24 h, are viable 100 %, as shown in **Figures 10(a)** and **10(b)**. The morphological microstructure (100×) is observed using an Olympus IX51 inverted fluorescence microscope. Recording the viability for each plate at a different point, After 60 min as shown in **Figure 11**, shows the viability for the mononuclear cells after incubation with NP in the dilatation 20, 50, 80, 110 and 140 mg/mL. Cell viability results ensure GT @Fe_3O_4 NP_S is blood biocompatibility, so it will be completely safe within few hours before any interaction with normal cells occurs. The blood biocompatibility of GT @Fe_3O_4 NP_S may relate to its surface nature. As the protective corrosivity of Fe_3O_4 is more than other Fe Oxides according to Pilling-Bedworth Ratio that is 1.9 [60]. Pilling-Bedworth Ratio depends on the percentage of oxides on the surface responsible for the protective layer.

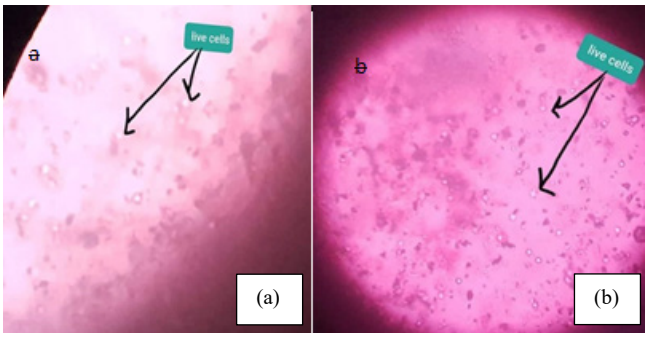

Figure 10 (a) The mononuclear cells after insulation 100 % viable (living) cells score, (b) The mononuclear cells after 24 h incubation 100 % viable (living) cells score.

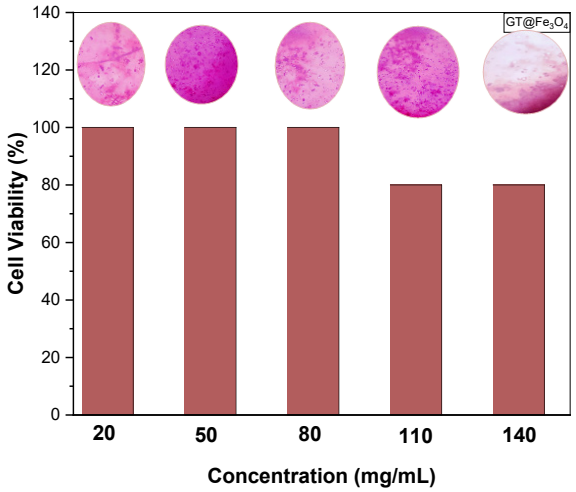

Figure 11 The mononuclear cells after incubation with NP in the dilatation 20, 50, 80, 110 and 140 mg/mL after 60 min.

Automatic coagulation analyzer

Prothrombin time (PT) is an essay evaluating the extrinsic pathway and common coagulation pathway. They are used to determine the clotting tendency of blood platelet. The poor plasma produced from a citrated blood sample is usually tested. It is worth noting that the GT@ Fe_3O_4 has far greater anticoagulant efficiency than heparin. Prothrombin time (PT) values of the GT@ Fe_3O_4 (14.50, 15.20 s) are higher than those of the lithium citrate (13.80 s), respectively **Figure 13**. The influences of the assembly time and particle clustering concentration on the clotting times were also investigated. The assembly time of GT@ Fe_3O_4 was found to have a much lower influence on the clotting times **Figure 14**, proving that the current approach to designing magnetic coagulants is efficient by coating Fe_3O_4 with green tea. As expected, the increased concentration of GT@ Fe_3O_4 highly improves the clotting times, As the clot prevention becomes more robust with increasing magnetic particle density.

As shown in **Figure 13**, PT of plain tube exceeds the limit time of the detector, as the blood in it is free of any additives, so the level of factors decreased attributed to blood clotting. On the other hand, PT of (Tube 2) with Heparin additives exceeds the maximum time as it consummates most extrinsic factors. Fe_3O_4 MNPs compensated some Prothrombin common factors. This table shows the delayed coagulation time as assessed by PT due to the consumption of coagulation factors by MNP_S. Thus, Fe_3O_4@GT NP_S was developed as an effective nano-anticoagulant for hemodialysis.

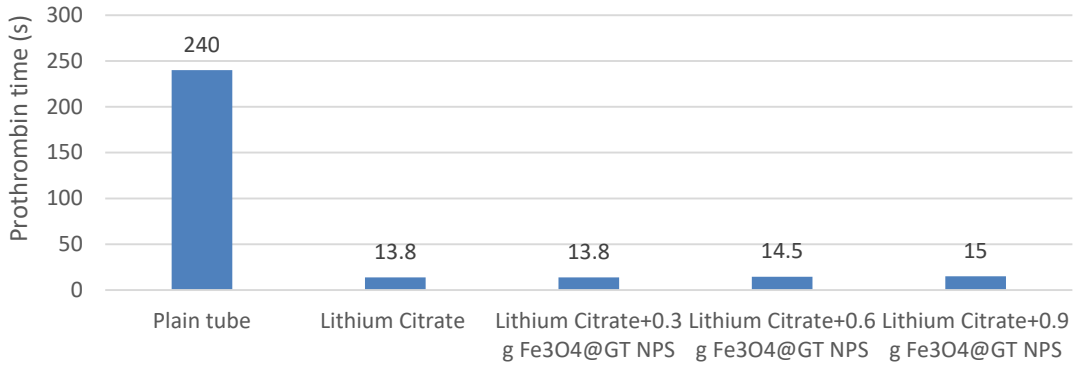

Figure 13 Comparison of PT for plain tube, heparin and GT@$Fe_3O_4NP_S$.

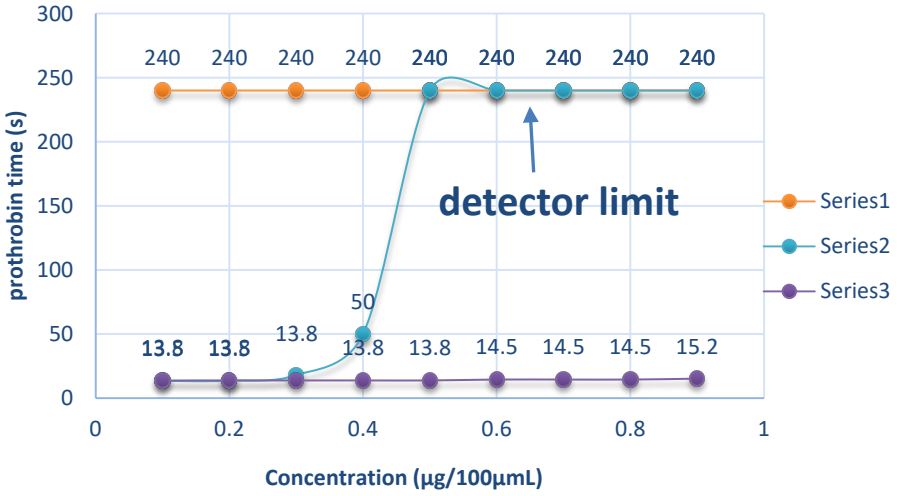

Figure 14 PT of plain tube, heparin and GT@$Fe_3O_4NP_S$.

Conclusions

As we showed in this study that our material GT@ Fe_3O_4 NP_S is entirely safe in living cells and has no side effects, so we can use it as a safe substitutional of heparin. Sample formed mainly from iron oxide as UV–V absorption spectrum of iron oxide nanoparticles GT@ Fe_3O_4 NPs displayed a peak in the region of 422.00 and 242 nm. X-ray diffraction patterns of the magnetite nanoparticles revealed diffraction peaks at which are the characteristic peaks of the Fe_3O_4 with a cubic spinel structure of Fe_3O_4-NPs that had been synthesized. FT-IR analysis shows 2 absorption bands between 400 and 630 cm^{-1}, which are the characteristic absorption peaks of Fe-O vibration related to Fe_3O_4 The presence of these functional groups (C–H stretching vibrations, C = N stretching, carbonyl groups C = C) confirmed that flavonoid and terpenoids molecules coated the surface of Fe_3O_4. TEM image displayed the synthesized Fe_3O_4-NPs mainly were spherical with an average size of 28 nm to 36 nm. The DLS measurements for the sample are performed in aqueous suspensions that displayed polydispersive behavior. The average size of MNPs obtained by DLS is higher than that observed in TEM, possibly due to the aggregation of MNPs in solution. The zeta potential for the sample is about 41.4 mV evidence greenly synthesized MNPs exhibit good colloidal stability due to coating with GT. Our results showed that magnetic GT@ Fe_3O_4 NPs could be a safe substitutional of heparin, overcoming side effects of heparin such as bleeding. GT@ Fe_3O_4 NPs can advance anticoagulant drugs by increasing control of the anticoagulant (e.g., decreasing the dose and reducing side effects while maintaining efficacy and increasing circulation). The new magnetic anticoagulant drugs will profit patients undergoing high-risk surgical procedures and overcome

anticoagulant-related bleeding problems to a great extent. In this work, we had some limitations related to the amount of sample, so we recommend test other higher concentrations in the anticoagulant assays. Assay the potential to use it as an anticoagulant drug invivo in an animal model. In the future, we expect magnetic nanoparticles will offer a strategy to treat thromboembolic events efficiently with the aid of Magnetic Resonance Imaging, as can serve as a negative contrast agent.

Acknowledgements

A patent was registered at the Egyptian Patent Office at the Ministry of Higher Education, Egypt under No 1286/2021.

References

[1] W Zhao, Q Liu, X Zhang, B Su and C Zhao. Rationally designed magnetic nanoparticles as anticoagulants for blood purification. *Colloid. Surface. B Biointerfac.* 2018; **164**, 316-23.

[2] W Zhao, RJ Yang, TT Qian, X Hua, WB Zhang and W Katiyo. Preparation of novel poly (hydroxyethyl methacrylate-co-glycidyl methacrylate)-grafted core-shell magnetic chitosan microspheres and immobilization of lactase. *Int. J. Mol. Sci*. 2013; **14**, 12073-89.

[3] AD Aderibigbe, RA Crane, MR Lees and AJ Clark. Selective uptake of Ag (I) from aqueous solutions using ionic liquid-modified iron oxide nanoparticles. *J. Nanopart. Res*. 2020; **22**, 216.

[4] N Boda, KCB Naidu, K MujasamBatoo, GHR Joice, JL Naik and D Ravinder. Structural, morphological and electronic properties of cadmium cobalt ferrite nanoparticle. Biointerface research in applied chemistry. *Islamic Azad Univ*. 2017; **6**, 2253-62.

[5] A Farnaz, H Jafarizadeh-Malmiri, H Ajamein, N Anarjan, H Vaghari, Z Sayyar and A Berenjian. A biotechnological perspective on the application of iron oxide nanoparticles. *Nano Resh*. 2016; **9**, 2203-25.

[6] S Kumar, R Singh, T Singh and A Batish. Investigations for magnetic properties of PLA-PVC-Fe_3O_4-wood dust blend for self-assembly applications. *J. Thermoplastic Compos. Mater*. 2019; **7**, 2021.

[7] Z Hou, Y Liu, J Xu and J Zhu. Surface engineering of magnetic iron oxide nanoparticles by polymer grafting: Synthesis progress and biomedical applications. *Nanoscale* 2020; **12**, 14957-75.

[8] M Javadi, VA Ortega, A Thiessen, M Aghajamali, MA Islam, JM Drummond, GG Goss and JGC Veinot. Cellular uptake and magneto-hyperthermia induced cytotoxicity using photoluminescent Fe_3O_4 nanoparticle/Si quantum dot hybrids. *ChemRxiv* 2020, DOI: 10.26434/chemrxiv.13138427.v1

[9] YP Yew, K Shameli, SE Mohamad, KX Lee and SY Teow. Green synthesized montmorillonite/carrageenan/Fe_3O_4 nanocomposites for pH-responsive release of protocatechuic acid and its anticancer activity. *Int. J. Mol. Sci.* 2020; **21**, 4851.

[10] JT Batley, M Nguyen, I Kamboj, C Korostynski, ES Aydil and C Leighton. Quantitative understanding of superparamagnetic blocking in thoroughly characterized Ni nanoparticle assemblies. *Chem. Mater.* 2020; **32**, 6494-506.

[11] RG Kerry, KE Ukhurebor, S Kumari, GK Maurya, S Patra and B Panigrahi. A comprehensive review on the applications of nano-biosensor based approaches for non-communicable and communicable disease detection. *Biomater. Sci.* 2021; **9**, 3476-602.

[12] H Alijani, A Noori, N Faridi, SZ Bathaie and MF Mousavi. Aptamer-functionalized Fe_3O_4@ MOF nanocarrier for targeted drug delivery and fluorescence imaging of the triple-negative MDA-MB-231 breast cancer cells. *J. Solid State Chem.* 2020; **292**, 121680.

[13] Y Qi, Y Du, J Tian, Z Jin and Y Li. *Antigen-loaded Fe_3O_4 nanoparticles for the stimulation and tracking of dendritic cell based vaccine.* American Association for Cancer Research, Philadelphia, 2020.

[14] M Suleman and S Riaz. 3D in silico study of magnetic fluid hyperthermia of breast tumor using Fe_3O_4 magnetic nanoparticles. *J. Therm. Biol*. 2020; **91**, 102635.

[15] RA Gabal, RM Shalaby, A Abdelghany and M Kamal. Antimicrobial effect, electric and structural correlation of nano-filled Tin Bismuth metal alloys for biomedical application. *Biointerface Res. Appl. Chem*. 2019; **9**, 4340-4.

[16] RB Onyancha, UO Aigbe, KE Ukhurebor and PW Muchiri. Facile synthesis and applications of carbon nanotubes in heavy-metal remediation and biomedical fields: A comprehensive review. *J. Mol. Struct*. 2021; **1238**, 130462.

[17] SM Taghizadeh, A Taherpoor and A Ebrahiminezhad. Algae and microalgae mediated synthesis of iron nanoparticles and their applications. *J. Adv. Med. Sci. Appl. Tech*. 2020; **5**, 1-11.

[18] S Parveen, AH Wani, MA Shah, HS Devi, MY Bhat and JA Koka. Preparation, characterization and antifungal activity of iron oxide nanoparticles. *Microb. Pathog.* 2018; **115**, 287-92.
[19] P Senthilkumar, S Babu, V Jaishree, KJ Stephen, G Yaswant, DSRS Kumar and NS Nair. Solvothermal-assisted green synthesis of hybrid Chi-Fe_3O_4 nanocomposites: A potential antibacterial and antibiofilm material. *IET Nanobiotechnol.* 2020; **14**, 714-21.
[20] A Rostami-Vartooni, A Moradi-Saadatmand, M Bagherzadeh and M Mahdavi. Green synthesis of $Ag/Fe_3O_4/ZrO_2$ nanocomposite using aqueous Centaurea cyanus flower extract and its catalytic application for reduction of organic pollutants. *Iranian J. Catal.* 2019; **9**, 27-35.
[21] J Choi, S Han, KT Nam and Y Seo. Hierarchically structured Fe_3O_4 nanoparticles for high-performance magnetorheological fluids with long-term stability. *ACS Appl. Nano Mater.* 2020; **3**, 10931-40.
[22] SA Fahmy, E Preis, U Bakowsky and HMES Azzazy. Palladium nanoparticles fabricated by green chemistry: Promising chemotherapeutic, antioxidant and antimicrobial agents. *Materials* 2020; **13**, 3661.
[23] SM Taghizadeh, A Zare-Hoseinabadi, A Berenjian, Y Ghasemi and A Ebrahiminezhad. Effective parameters in the green synthesis of zero-valent iron nanoparticles as a fenton-like catalyst. *J. Environ. Treat. Tech*. 2020; **8**, 442-7.
[24] I Hussain, N Singh, A Singh, H Singh and S Singh. Green synthesis of nanoparticles and its potential application. *Biotechnol. Lett.* 2016; **38**, 545-60.
[25] F Namvar, R Mohamad, J Baharara, S Zafar-Balanejad, F Fargahi and HS Rahman. Antioxidant, antiproliferative, and antiangiogenesis effects of polyphenol-rich seaweed (*Sargassum muticum*). *BioMed Res. Int*. 2013; **2013**, 604787.
[26] F Namvar, HS Rahman, R Mohamad, J Baharara, M Mahdavi, E Amini, MS Chartrand and SK Yeap. Cytotoxic effect of magnetic iron oxide nanoparticles synthesized via seaweed aqueous extract. *Int. J. Nanomed.* 2014; **9**, 2479-88.
[27] GE Hoag, JB Collins, JL Holcomb, JR Hoag, MN Nadagouda and RS Varma. Degradation of bromothymol blue by 'greener' nano-scale zero-valent iron synthesized using tea polyphenols. *J. Mater. Chem.* 2009; **19**, 8671-7.
[28] T Shahwan, SA Sirriah, M Nairat, E Boyacı, AE Eroğlu, TB Scott and KR Hallam. Green synthesis of iron nanoparticles and their application as a fenton-like catalyst for the degradation of aqueous cationic and anionic dyes. *Chem. Eng. J.* 2011; **172**, 258-66.
[29] T Wang, X Jin, Z Chen, M Megharaj and R Naidu. Green synthesis of Fe nanoparticles using eucalyptus leaf extracts for treatment of eutrophic wastewater. *Sci. Total Environ.* 2014; **466**, 210-3.
[30] MF Vitha. *Spectroscopy: Principles and instrumentation*. John Wiley & Sons, New Jersey, 2018.
[31] R Upadhyay, K Davies, S Wells and S Charles. Preparation and characterisation of ultra-fine MnFe2O4 and MnxFe1-xO4 spined systems: II. Magnetic fluids. *J. Magn. Magn. Mater*. 1995; **139**, 249-54.
[32] B Abdullah and D Tahir. Quantitative analysis of x-ray diffraction spectra for determine structural properties and deformation energy of Al, Cu and Si. *J. Phys. Conf. Ser.* 2019; **1317**, 012052.
[33] MA Mohamed, J Jaafar, AF Ismail, MHD Othman and MA Rahman. *Fourier transform infrared (FTIR) spectroscopy*. *In*: N Hilal, AF Ismail, T Matsuura and D Oatley-Radcliffe (Eds.). Membrane Characterization. Elsevier, Amsterdam, Netherlands, 2017, p. 3-29.
[34] M Kannan. *Transmission electron microscope-principle, components and applications illumination system (electron gun and condenser lenses) electron gun*. *In*: M Kannan (Ed.). A textbook on fundamentals and applications of nanotechnology. DAYA Publishing House, Delhi, India, 2018, p. 93-101.
[35] MS El-Eskandarany. *Characterizations of mechanically alloyed powders. In*: MS El-Eskandarany (Ed.). Mechanical Alloying. 3rd (ed). William Andrew Publishing, Norwich, NY, 2020, p. 13-8.
[36] H El-Kassas, MA Aly-Eldeen and S Gharib. Green synthesis of iron oxide (Fe_3O_4) nanoparticles using two selected brown seaweeds: Characterization and application for lead bioremediation. *Acta Oceanol. Sin.* 2016; **35**, 89-98.
[37] T Shahwan, S Abu Sirriah, M Nairat, E Boyacı, AE Eroğlu, TB Scott and KR Hallam. Green synthesis of iron nanoparticles and their application as a fenton-like catalyst for the degradation of aqueous cationic and anionic dyes. *Chem. Eng. J*. 2011; **172**, 258-66.
[38] R O'brien, D Cannon and W Rowlands. Electroacoustic determination of particle size and zeta potential. *J. Colloid. Interface Sci.* 1995; **173**, 406-18.
[39] P Marcon and K Ostanina. Overview of methods for magnetic susceptibility measurement. *In*: Proceedings of the Progress in Electromagnetics Research Symposium Proceeding, Kuala Lumpur,

Malaysia. 2012.
[40] T El-Alaily, M El-Nimr, S Saafan, M Kamel, T Meaz and S Assar. Construction and calibration of a low cost and fully automated vibrating sample magnetometer. *J. Magn. Magn. Materials* 2015; **386**, 25-30.
[41] C Yeo, N Saunders, D Locca, A Flett, M Preston, P Brookman, B Davy, A Mathur and S Agrawal. Ficoll-Paque versus Lymphoprep: A comparative study of two density gradient media for therapeutic bone marrow mononuclear cell preparations. *Regen. Med.* 2009; **4**, 689-96.
[42] SM Taimoory, JF Trant, A Rahdar, M Aliahmad, F Sadeghfar, M Hashemzaei. Importance of the inter-electrode distance for the electrochemical synthesis of magnetite nanoparticles: synthesis, characterization, computational modelling, and cytotoxicity. *E-J Surf. Sci. Nanotech.* 2017; **15**, 31-9.
[43] A Woolley, JL Golmard and S Kitchen. Effects of haemolysis, icterus and lipaemia on coagulation tests as performed on Stago STA-compact-max analyser. *Int. J. Lab. Hematol.* 2016; **38**, 375-88.
[44] P Makuła, M Pacia and W Macyk. How to correctly determine the band gap energy of modified semiconductor photocatalysts based on UV-vis spectra. *J. Phys. Chem. Lett.* 2018; **9**, 6814-7.
[45] I Kazeminezhad and S Mosivand. Phase transition of electrooxidized Fe_3O_4 to γ and α-Fe_2O_3 nanoparticles using sintering treatment. *Acta Phys. Pol. A* 2014; **125**, 1210-4.
[46] M Kamal, R Abogabil, EE Al-Wakeel, AER MM and K Shalabi. The physical and biological properties of alkali - Heat treated titanium implant material. *Int. J. Eng. Tech.* 2013.
[47] X Zhang, S Lin, Z Chen, M Megharaj and R Naidu. Kaolinite-supported nanoscale zero-valent iron for removal of Pb^{2+} from aqueous solution: Reactivity, characterization and mechanism. *Water Res*. 2011; **45**, 3481-8.
[48] W Li, D Liu, J Wu, C Kim and JD Fortner. Aqueous aggregation and surface deposition processes of engineered superparamagnetic iron oxide nanoparticles for environmental applications. *Environ. Sci. Tech*. 2014; **48**, 11892-900.
[49] HK Can, S Kavlak, S ParviziKhosroshahi, A Güner. Preparation, characterization and dynamical mechanical properties of dextran-coated iron oxide nanoparticles (DIONPs). *Artif. Cell. Nanomed. Biotechnol.* 2018; **46**, 421-31.
[50] AM Awwad and NM Salem. A green and facile approach for synthesis of magnetite nanoparticles. *Nanosci. Nanotechnol.* 2012; **2**, 208-13.
[51] G Vázquez, E Fontenla, J Santos, M Freire, J González-Álvarez and G Antorrena. Antioxidant activity and phenolic content of chestnut (*Castanea sativa*) shell and eucalyptus (*Eucalyptus globulus*) bark extracts. *Industrial crops and products*. 2008; **28**, 279-85.
[52] K Singh, K Senapati and K Sarma. Synthesis of superparamagnetic Fe_3O_4 nanoparticles coated with green tea polyphenols and their use for removal of dye pollutant from aqueous solution. *J. Environ. Chem. Eng.* 2017; **5**, 2214-21.
[53] G Parshetti, A Telke, D Kalyani and S Govindwar. Decolorization and detoxification of sulfonated azo dye methyl orange by Kocuria rosea MTCC 1532. *J. Hazard. Mater.* 2010; **176**, 503-9.
[54] HI Saleh. Green synthesis of magnetite nanoparticles using *Myrtuscommunis*L. Grown in Egypt. *Int. Res. J. Innovat. Eng. Tech.* 2017; **4**, 6-13.
[55] AN Ilinskaya and MA Dobrovolskaia. Nanoparticles and the blood coagulation system. Part I: benefits of nanotechnology. *Nanomedicine* 2013; **8**, 773-84.
[56] NK Verma, K Crosbie-Staunton, A Satti, S Gallagher, KB Ryan, T Doody, C McAtamney, R MacLoughlin, P Galvin, CS Burke, Y Volkov and YK Gun'ko. Magnetic core-shell nanoparticles for drug delivery by nebulization. *J. Nanobiotechnol*. 2013; **11**, 1.
[57] Q Peng, S Zhang, Q Yang, T Zhang, X-Q Wei, L Jiang, CL Zhang, QM Chen, ZR Zhang and YF Lin. Preformed albumin corona, a protective coating for nanoparticles based drug delivery system. *Biomaterials* 2013; **34**, 8521-30.
[58] M Anand. Hysteresis in a linear chain of magnetic nanoparticles. *J. Appl. Phys.* 2020; **128**, 023903.
[59] EA Hassan, N Nawar and MM Mostafa. Comparative studies of some novel Cu^{2+} and Fe^{3+} chelates derived from tricine (L1) by single crystal x-ray, spectroscopic and biological data: Applications to investigate antitumor activity. *Appl. Organomet. Chem.* 2019; **33**, 5096.
[60] C Xu and W Gao. Pilling-bedworth ratio for oxidation of alloys. *Mater. Res. Innovat*. 2000; **3**, 231-5.